Wettability modification of laser-fabricated hierarchical surface structures in Ti-6Al-4V titanium alloy

Huerta-Murillo, Daniel; Garcia Giron, Antonio; Romano, Jean-Michel; Cardoso, José T.; Cordovilla, F. ; Walker, Marc ; Dimov, Stefan; Ocaña, José L.

DOI:
10.1016/j.apsusc.2018.09.012

Accepted Manuscript

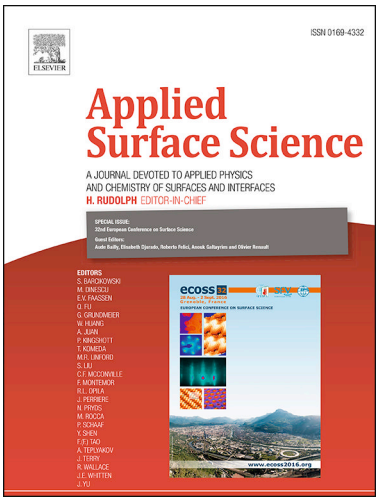

Full Length Article

Wettability modification of laser-fabricated hierarchical surface structures in Ti-6Al-4V titanium alloy

D. Huerta-Murillo, A. García-Girón, J.M. Romano, J.T. Cardoso, F. Cordovilla, M. Walker, S.S. Dimov, J.L. Ocaña

PII: S0169-4332(18)32424-3
DOI: https://doi.org/10.1016/j.apsusc.2018.09.012
Reference: APSUSC 40316

To appear in: *Applied Surface Science*

Received Date: 18 May 2018
Revised Date: 7 August 2018
Accepted Date: 1 September 2018

Please cite this article as: D. Huerta-Murillo, A. García-Girón, J.M. Romano, J.T. Cardoso, F. Cordovilla, M. Walker, S.S. Dimov, J.L. Ocaña, Wettability modification of laser-fabricated hierarchical surface structures in Ti-6Al-4V titanium alloy, *Applied Surface Science* (2018), doi: https://doi.org/10.1016/j.apsusc.2018.09.012

Wettability modification of laser-fabricated hierarchical surface structures in Ti-6Al-4V titanium alloy.

D. Huerta-Murillo [a, *] · A. García-Girón [b] · J. M. Romano [b] · J. T. Cardoso [a] · F. Cordovilla [a] · M. Walker [c] · S.S. Dimov [b] · J. L. Ocaña [a]

[a] *UPM Laser Centre, Polytechnical University of Madrid, Ctra. Valencia km 7.3, 28031, Madrid, Spain*
[b] *School of Mechanical Engineering, University of Birmingham, Edgbaston, Birmingham, B15 2TT, UK*
[c] *Department of Physics, University of Warwick, Coventry, CV4 7AL, UK*
** Corresponding author: D. Huerta-Murillo. E-mail address: d.huerta@upm.es*

ARTICLE INFO

Received:
Accepted:
Available:

Keywords:

Laser Material Processing
Periodic Surface Structures
Ti-6Al-4V
Direct Laser Writing
LIPSS

ABSTRACT

In the present work, a study of laser-based surface structuring of aerospace-grade titanium alloy (Ti-6Al-4V) with subsequent ageing by employing two different storage methods is undertaken. The titanium alloy samples were patterned using UV-ns and IR-fs pulsed lasers in a two-step process to fabricate bio-inspired hierarchical structures. The resulting surface structure consisted in regular periodic square-shaped micro-pillars covered by 810 nm-periodic LIPSS. After the laser processing the samples were kept in two different storage conditions: exposed to ambient air and inside polyethylene bags. The polyethylene bags were found to be beneficial for the surface ageing of laser-fabricated titanium surfaces, increasing the ageing time when compared to ageing by exposure to ambient air. Hierarchical surface topographies exhibited higher water-repellency when compared to non-hierarchical structures. Especially, hierarchical structures reached a hydrophobic state with water contact angle over 160° after 3 weeks storage in polyethylene bags. The micro-structured surfaces were characterized by using confocal microscopy, scanning electron microscopy, static contact angle measurements and X-ray photoelectron spectroscopy.

1. Introduction

Nature has always inspired the development of tools and it has been a source of innovations and solutions to several technological problems in many fields. In the material surfaces field, bio-inspired functional surfaces have been a very active research topic in recent years in order to mimic some of the properties that are shown on certain natural surfaces [1,2]. Specifically, the “lotus-effect” is a well know example of a natural hydrophobic behavior, in which water droplets hardly wets the surface of the lotus leaf allowing the water droplets to easily roll-off the surface, removing contaminating particles along its path and thus creating a self-cleaning effect. It has been shown that the surface topography of the lotus leaves exhibits a dual-scale roughness structure, i.e., micro-scale structures are covered by nano-scale features, and that this unique roughness configuration is strongly related to the hydrophobicity of the lotus leaf [3–5]. Several theories and models had been proposed to explain the way that droplets interact with the surface in order to find a suitable surface roughness with a high hydrophobicity [6–8]. In a simplified manner, to achieve a good hydrophobic state, when a water droplet gets into contact with a dual-scale surface, the droplet must make contact only with some fraction of the surface due to the nano- and micro-scale features, leaving air trapped between the droplet-surface interfaces. The

droplet then is supported by a composite interface of material surface and air, a state defined by the Cassie-Baxter model [9].

To achieve this dual-scale surface roughness, chemical and mechanical methods have been proposed to modify the surface and improve the wettability behavior [10–12]. Among these methods, direct laser writing (DLW) with short and ultra-short pulsed lasers has been investigated due to several characteristics and advantages of the laser micro-machining process. Advantages of this approach include non-chemical contamination and being able to achieve a wide range of structures with several geometries in the nano- and micro-scale with a high localized precision. DLW has proven to be a very good technique for material processing with a great range of applications [13–15]. Direct laser processing facilitates the removal of a controlled volume of material through an ablation process or allows only to modify the surface without material removal using continuous wave laser or short- and ultra-short pulsed laser. Specifically, with regards to wettability, several types of structures generated by laser material processing have been reported on a variety of materials, showing changes to the wettability of the surfaces, either achieving hydrophobic or hydrophilic states [16–19].

In the case of short-pulsed lasers (nanosecond pulses), which are an effective and low-cost process for material micro-machining, a great progress has been achieved in producing hydrophobic surfaces with ns-sources for several applications like enhanced corrosion properties [20,21], improved durability under abrasive wear with self-healing properties on stainless steel using chemical coating [22] or homogeneous spot deposition of polystyrene particles [23], all this application make the nanosecond patterned surfaces a very promising technology for the creation of functional surfaces at an industrial level. Nevertheless, the nanosecond laser process is accompanied by strong thermal effects and melted material may re-solidified on the periphery of the laser irradiated zones, being this an important limitation when creating patterned surfaces with high precision. However, this characteristic recast of material when working with nanosecond lasers have been proven to have an advantageous effect when creating hydrophobic surfaces [16,24,25].

Also, a spatial limitation in the dimensions of the structures that can be achieved by nanosecond ablation is encountered, since the minimum structure dimensions are in the micro-scale and is determined by the beam spot diameter. This limitation can be avoided by using ultra-short laser pulses (picosecond and femtosecond pulses), which have been proven to create sub-micron structures in a very uniform manner with minimal thermal effects.

Among the different types of surface structures that have been reported after ultra-short pulsed laser irradiation, laser-induced periodic surface structures (LIPSS) have gained a lot of attention in the recent years due to their potential applications for surface functionalization. These periodic structures consist usually in long parallel ripples extended over the irradiated zones, with typical dimensions on the nano-scale, and with a periodicity that is always much lower (high spatial frequency LIPSS, HSFL) or close to (low spatial frequency LIPSS, LSFL) the laser wavelength used for the laser process. The formation of LIPSS have been investigated for several applications, including decorative purposes due to diffraction from the surface, anti-icing or self-cleaning applications [26–28]. Recently, multi-step processes have been developed combining different laser marking techniques to generate hierarchical structures on the surfaces of different materials, in some cases achieving enhanced hydrophobic effects, useful because of the wide range of potential applications for hydrophobic surfaces [29,30]. However, the wettability of a surface is not only influenced by the surface roughness but also by the chemical composition [31,32]. It

has been shown that structured surfaces undergo a change in their chemical composition due to ageing, potentially leading to a transition between hydrophilic and hydrophobic states [16,33,34]. This aging process depends largely on the laser source and patterning process, subsequent storage conditions and the initial composition of the material itself.

In this article we report on an investigation in to the wetting behavior of laser textured surfaces of aerospace grade Ti-6Al-4V alloy. The samples were processed with a two-step laser approach, combining DLW with nanosecond and LIPSS (in particular LSFL) with femtosecond pulsed laser sources. Hierarchical structures were fabricated in order to evaluate the potential of dual-scale micro and nano topographies for hydrophobic surfaces. Additionally, the aging of the laser-textured surfaces and the role of storage conditions in ambient air and polyethylene $(C_2H_4)_n$ bags were investigated.

2. Material and methodology

2.1 Material

Ti-6Al-4V sheets (2 mm thick) with an initial surface roughness of S_a = 452 nm were used for laser surface micro-structuring via direct laser writing. The surface of the material was structured via laser ablation without any prior process on the samples, apart from cleaning with ethanol before the laser processing. After laser processing, the samples were kept, without further treatment, in two different storage conditions for several weeks: ambient air and polyethylene $(C_2H_4)_n$ bags, both subjected to lab conditions under atmospheric pressure and room temperature.

2.2 Laser system and processing parameters

A Spectra-Physics solid-state pulsed nanosecond laser source was used to perform the laser processing of the samples. The pulses generated by the source had a Gaussian profile with a fixed duration of 30 nanoseconds, an average power of 20 W at a repetition rate of 100 kHz and a wavelength of 355 nm. The laser beam was focused onto the sample at normal incidence with a 250-mm focal lens to generate a spot size of 15 µm. The position of the sample was controlled using a translational stage using a fixed scan speed of 80 mm/s.

The laser machining process consisted of creating surfaces structured with square-shaped micro-pillars via laser ablation. The desired geometry consisting of an array of micro-pillars was achieved after etching cross-like micro-channels on the sample. The separation of the micro-channels was the same in both directions of the laser scanning and is henceforth referred to as the Hatch Distance (H.D.). This hatch distance determines the spatial length of the micro-pillar. Surfaces areas of 1x1 cm were patterned with nine different laser power values. The process parameters used for the fabrication of the micro-cells are shown in Table 1.

Table 1.: Laser processing parameters for the fabrication of micro-cells on Ti-6Al-4V via DLW technique.

Pulse fluence (J/cm^2)	0.08 – 1.64
Repetition Rate (kHz)	100
Scan Speed (mm/s)	80

Hatch Distance (H.D.) (µm)	20
Beam spot size (µm)	15

Inspired by natural hydrophobic surfaces, a dual-scale surface roughness was created in a two-step laser patterning process, using a second laser source (fs), to investigate the contribution of LIPSS in the hydrophobicity of the material when compared with the micro-structures fabricated with ns laser. Using a femtosecond pulsed laser source with an average power of 5 W and linear polarization, 310 fs pulse duration, a central wavelength in the near-infrared domain of 1032 nm and a repetition rate that can be tuned to a chosen value by means of an external modulator (MOD) that is controlled by the software of the system. The system allows to select a repetition rate (f) from a maximum of 500 kHz and down to any value of f/N (N being an integer), IR-fs LIPSS were formed on top of the UV-ns micro-pillars. The laser system used a galvo scanner with a 3D scan head and a 100-mm focal length telecentric lens to deflect the laser beam at normal incidence to the sample. The laser beam had a Gaussian profile and a spot diameter of approximately 35 µm at focus. Laser processing was performed in atmospheric conditions and cleaned by compressed air. The process parameters used for the fabrication of the IR-fs LIPSS are shown in Table 2.

Table 2.: Laser processing parameters for the fabrication of IR-fs LIPSS on Ti-6Al-4V via DLW.

Pulse Energy (µJ)	1.1
Repetition Rate (kHz)	100
Scan Speed (mm/s)	500
Hatch Distance (H.D.) (µm)	5
Beam spot size (µm)	15

2.3 Characterization

Characterization of the samples was performed to evaluate the topography, wettability and chemical composition of the laser-structured and bare surfaces. The surfaces topographies were examined using scanning electron microscopy (SEM, HITACHI S-3000N) and confocal laser microscopy (Leica DCM 3D).

The wettability behavior of the structures was evaluated via static contact angle (SCA) measurements, using a sessile drop technique along with a video-based optical contact angle measuring system. Milli-Q water droplets with a volume of 10 µl were dispensed in air conditions for all the measurements. The SCA was obtained by analyzing images of the droplets on the surface of the sample captured by the camera after being dispensed. Additionally, the contact angle hysteresis values were measured. Posterior to the measurements samples were cleaned using compressed air.

Furthermore, X-ray photoelectron spectroscopy (XPS) was performed to evaluate the chemical composition of nano-second DLW processed samples stored in two different conditions. The samples were mounted on a sample bar of a Kratos Axis Ultra DLD spectrometer (Kratos Analytical, UK), with a base pressure of ~$2x10^{-10}$ mbar. A monochromated Al Kα X-ray source was used for the sample irradiation at room temperature. The XPS measurements were calibrated using the Fermi edge and $3d_{5/2}$

peak recorded from a polycrystalline Ag sample. The XPS spectra were recorded from an analysis area of 300 x 700 µm. The data was analyzed in the CasaXPS package using Shirley backgrounds and Voigt line shapes.

3. Results and discussion

3.1 UV-ns laser textured micro-structures

Cross-like micro-channels were patterned on the surface of Ti-6Al-4V samples via UV-ns direct laser writing. The cross-like channels created an array of square-shaped micro-pillars with a 20 µm hatch distance. With a fixed repetition rate of 100 kHz, nine different fluences were used to observe the difference on the topography. Fig. 1 shows an SEM micrograph of the different topographies obtained.

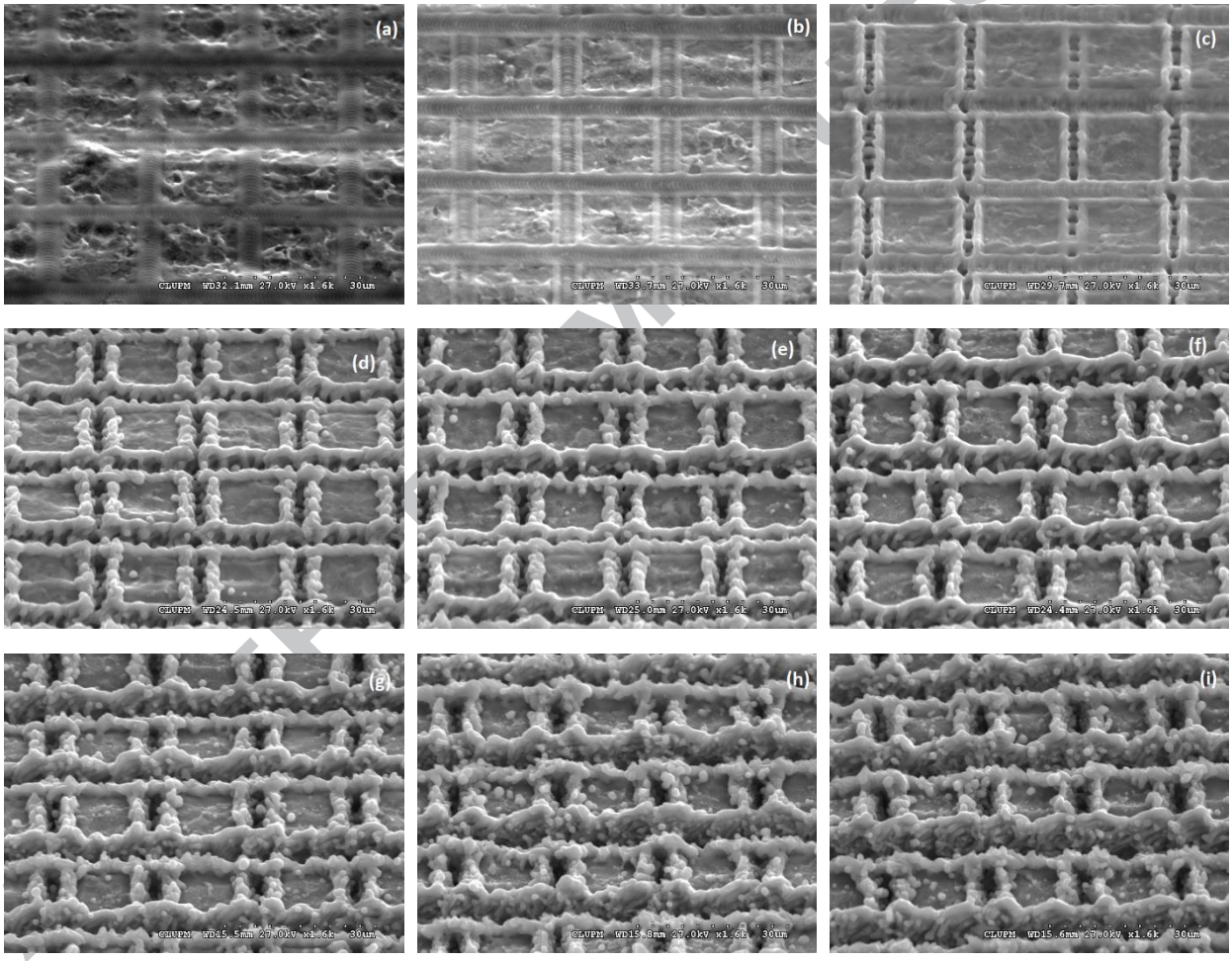

Fig. 1. Scanning electron micrographs of the top view of titanium alloy micro-structured surfaces showing periodic square-shaped micro-pillars for nine different avg. laser powers: a) 15 mW, b) 50 mw, c) 85 mW, d) 120 mW, e) 150 mW, f) 185 mW, g) 220 mw, h) 250 mW, i) 290 mW. (Scanning speed 80mm/s, 100 kHz repetition rate, H.D. 20 µm.)

For a very low laser power of 15 mW, the micrograph in Fig. 1.a shows that the surface has tracks slightly marked by the laser beam path, nevertheless, these tracks do not change the surface roughness in a considerable manner. As the power increases and due to the nature of the nanosecond pulses, the

surface was rapidly heated on the zone irradiated with a power higher than 50 mW, causing the material to melt and evaporate, creating deeper micro-channels by means of an ablation process as the laser scans the sample. The molten material was ejected because of the vapor pressure and began to accumulate along the sides of the micro-channels, creating a micro-wall with the recast of the molten material as it re-solidified along the laser path. For a laser power range between 150-220 mW, more material was melted and removed as the laser scan the surface and deeper micro-channels were created. The cross-like scanning process created clear micro-pillars with a considerable amount of recast material on the top which act as micro-walls around the original surface that has not been irradiated with laser pulses. The height of the micro-walls, as well as the depth of the micro-channels depends on the laser power as observed in Fig. 1. For the laser powers used in this work, the maximum height from the surface on the center of the pillars to the top of the wall and the maximum depth to the bottom of the channels was around 3 and 4 µm respectively. The micro-structures fabricated show strong evidence of thermal effects, becoming more visible as the laser power increases. Due to the increase of energy deposited on the surface, the temperature of the surface and the amount of melted material increases, giving rise to larger micro-walls when using higher power in comparison with the lower power values, for which the micro-pillars did not form properly as the material only got marked slightly, an effect similar to a laser polish. Additionally, for high powers, spherical-shaped particles can also be observed on the center of the micro-pillars because of metal vapor re-solidification as it can be observed on Fig. 1.g-h. Due to the laser beam spot size and the thermal effects that accompany nanosecond laser ablation, a spatial resolution limit is unavoidable when creating well organized surface micro-structures with the UV nanosecond laser system, in this case the limit was 15 µm.

3.2 Dual-scale hierarchical structures

Inspired in natural hydrophobic surfaces and trying to fabricate a hierarchical surface roughness, IR-fs low spatial frequency LIPSS were created on top of the prior micro-pillars to create laser induced dual-scale surface structures. Pulsed laser irradiations with a femtosecond pulsed laser source in the near-infrared were performed by means of an optimized laser process to generate large areas with LIPSS for which a detailed description has been reported previously [35] using the parameters shown in Table 2. The structuring process employs a high pulse-to-pulse overlap in the direction of the laser scan path, for the case of Ti-6Al-4V, 28 effective pulses per spot size were found to be necessary for LIPSS generation using a laser fluence per pulse of 0.16 J/cm^2, a scanning speed of 500 mm/s and a pulse repetition rate of 100 kHz. The resulting morphology can be seen on Fig. 2, which shows self-organized ripples in a very uniform manner with a spatial period of approximately 810 nm.

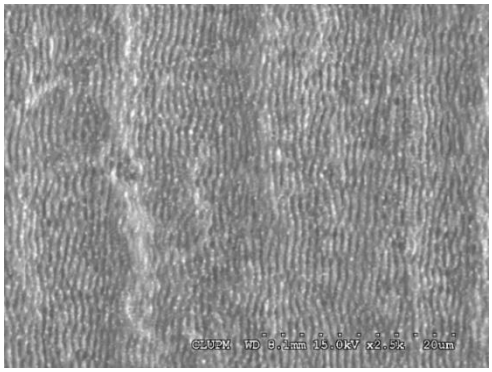

Fig. 2. SEM micro-graph of the IR-fs low spatial frequency LIPSS generated on Ti-6Al-4V surfaces (wavelength: 1032 nm, pulse duration: 310 fs, repetition rate: 100 kHz, pulse fluence: 0.16 J/cm^2, spatial period: 810 nm).

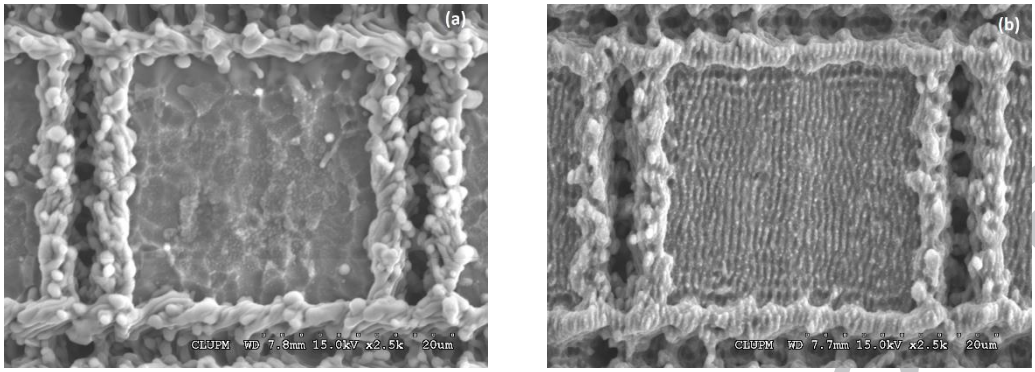

Fig. 3. SEM micrographs of the topographies on the surfaces of Ti-6Al-4V laser-patterned samples: (a) ns-DLW before LIPSS, (b) ns-DLW after LIPSS. (DLW structure: wavelength: 355 nm, pulse duration: 30 ns, repetition rate: 100 kHz, fluence: 5.65 J/cm^2, scan speed: 80 mm/s; LIPSS: wavelength: 1032 nm, pulse duration: 310 fs, repetition rate: 100 kHz, fluence: 0.16 J/cm^2, spatial period: 810 nm).

Hierarchical structures were generated by combining both UV-ns and IR-fs direct laser writing structures on the same surface. As can be observed on Fig. 3, the formation of IR-fs LIPSS did not destroy the previously patterned UV-ns micro-pillar, giving place to a well-defined dual-scale surface roughness. The IR-fs LIPSS can be observed both in the micro-walls and in the center of the micro-pillars in a very homogeneous way, showing also a smoother overall structure. These dual-scale topographies are expected to show a better wettability behavior in comparison with the single UV-ns micro-pillars due to the roughness inspired on natural hydrophobic surfaces.

3.3 Storage conditions and Wettability behavior

Generally, the wettability behavior of a material depends on both the surface topography and the chemical composition. It is reported in the literature that after a laser structuring process, ageing will affect the wettability behavior of the surfaces due to a chemical change of the surface composition. Furthermore, recently the role of storage conditions after the laser patterning for fabrication of hydrophobic surfaces has been studied [16,34]. This demonstrated that different storage conditions can affect the ageing process of micro-structured surfaces, either hastening or delaying the transition between hydrophilic and hydrophobic states. The fact that storage conditions may affect and change the chemical composition of the laser-patterned surfaces may be due to the chemical compounds to which the surface is exposed on the different storage conditions.

To analyze how the storage affects the ageing process and the wettability behavior of the Ti-6Al-4V patterned surfaces, two samples (processed with the same laser patterns) kept on two different storage conditions, ambient air and polyethylene $(C_2H_4)_n$ bags, were used to observe and compare the evolution of the SCA for several weeks. The static contact angle measurements were made using a sessile drop technique together with a video-based optical contact angle measuring system. Milli-Q water droplets with a volume of 10 µl were dispensed in air conditions. The reference non-processed surface recorded a SCA of approximately 70°, without any significant change due to the storage conditions. The processed samples were highly hydrophilic immediately after the laser micro-machining. The evolution of the contact angles for samples kept in different storage conditions are shown in Fig 4. These data clearly

demonstrate that samples stored in the polyethylene bags exhibit an increase in the contact angle after the first week in comparison to samples stored in air. After one month of storage, the samples stored in the bags shows an even clearer difference in comparison with the samples kept on air, reaching values over 150°. Since the surface topography was fabricated with the same parameters, the change in contact angles between the two storage conditions must be related to a change in the chemical composition of the surfaces, nevertheless, it cannot be denied that the micro-structures also play an important role in the transition between wettability states, since all the laser-patterned samples exhibit an improvement in the SCA values in both storage conditions when compared with the non-processed surfaces.

Additionally, dual-scale samples were also kept in two different storage conditions. SCA measurements for hierarchical structures and single-scale structures on both air and polyethylene bags storage are shown in Fig. 5. It can be observed that dual-scale hierarchical structures exhibit an improvement in SCA against non-hierarchical micro-pillars for samples stored in both air and polyethylene bags, this demonstrate that a hierarchical roughness leads to an increase in surface hydrophobicity. However, once again, samples that were kept in polyethylene bags exhibit a faster ageing process, achieving a hydrophobic state with higher SCA for the hierarchical structures in a shorter time period when compared to the one stored in a polyethylene bag. Once again, demonstrating that both induced roughness and chemical change play an important role in the wettability transition.

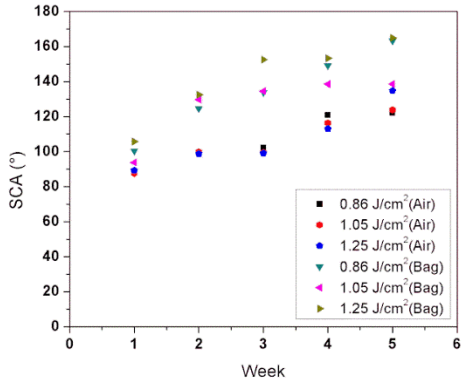

Fig. 4. Static contact angle values for UV-ns micro-pillars for three different laser fluences and two different storage conditions.

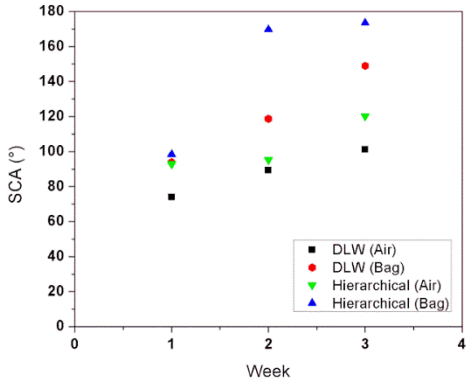

Fig. 5. Static contact angle values for micro-pillars as well as hierarchical pillars in two different storage conditions.

Additionally, the contact angle hysteresis values of the hierarchical and non-hierarchical (DLW) surfaces were measured for both air and bag storage. The values are above 20° for the four samples, meaning that they do not reach a hydrophobic state with good rolling-off effect for the water droplets deposited in the surface, nevertheless, the results of the SCA clearly show an improvement in the hydrophobicity when comparing the laser-patterned surfaces against un-processed surfaces. From these results, it is clear that a dual-scale or hierarchical surface structure is important to generate hydrophobic surfaces, as hierarchical structures show a higher SCA values in comparison to single-scale structures. Moreover, although the surface roughness can improve the wettability of the surface, the storage conditions and associated changes in the chemical composition of the surface must also play an important role as there is a difference in the SCA values for both the hierarchical and non- hierarchical structures kept in the two different storage conditions.

3.4 Chemical characterization

To study the consequence of the two different storage conditions on the final surface chemical composition and the relationship with surface wettability, the surfaces of the DLW nanosecond laser patterned samples stored in air and polyethylene bags were analyzed using X-ray photoelectron spectroscopy (XPS). The XPS survey spectra of the bare material and the nanosecond laser treated surfaces in the two storage conditions are shown in Fig. 6. For the non-processed surface, the main elements found were carbon and oxygen, this is expected mainly because of contamination and oxidation of the surface due to the water molecules and other atmospheric contaminants. In addition to the C 1*s* and O 1*s* peaks, the reference sample shows a very small peak on the Ti 2*p* region. The bare surface contained also negligible amounts of Al, Ca, S, Si, Cl, K, N and a strong Auger peak at ~497.0 eV corresponding to Na KLL Auger emission, which disappears after the laser process.

The XPS spectra and the detailed atomic elemental composition of the main elements found, summarized in Table 3, shows an increase in the percentage of titanium concentration in comparison with the bare material for the case of the laser patterned samples on both storage conditions, this may be attributed to the removal of contaminants in the surface as a result of the laser process, nevertheless, the concentration of Al did not change considerably. Furthermore, the concentration of carbon on the reference sample was very high whereas for the processed samples a clear decrease in the C concentration can be observed. Additionally, the XPS analysis showed that despite the laser treatment leading to the removal of hydrocarbons from the surface, the relative amount of oxygen increased after laser pattering, suggesting the presence of significant amounts of metal oxides on the surface. Additionally, due to contamination, the reference sample exhibit low concentration (>6.6%) of S, Cl, K, and Na, that are not detected on neither of the laser patterned samples. Also a small percentage of Si was detected (>2%); when found in high concentrations, the element Si must exhibit a peak on the XPS spectra around 103 eV, however, the concentration of Si found in all the samples does not account to exhibit a clear peak in Fig 6. The relative contribution of Ca is very similar for all samples, showing a very low concentration in comparison with the main elements found (<0.25%). Furthermore, no concentration of V was found in the reference sample due to contamination, yet a small concentration was found after the laser process (>0.4%). Lastly, N was found on the reference sample with a small contribution to the relative surface composition (>2.1%) and diminishes after the laser process for both storage conditions (>1.55%).

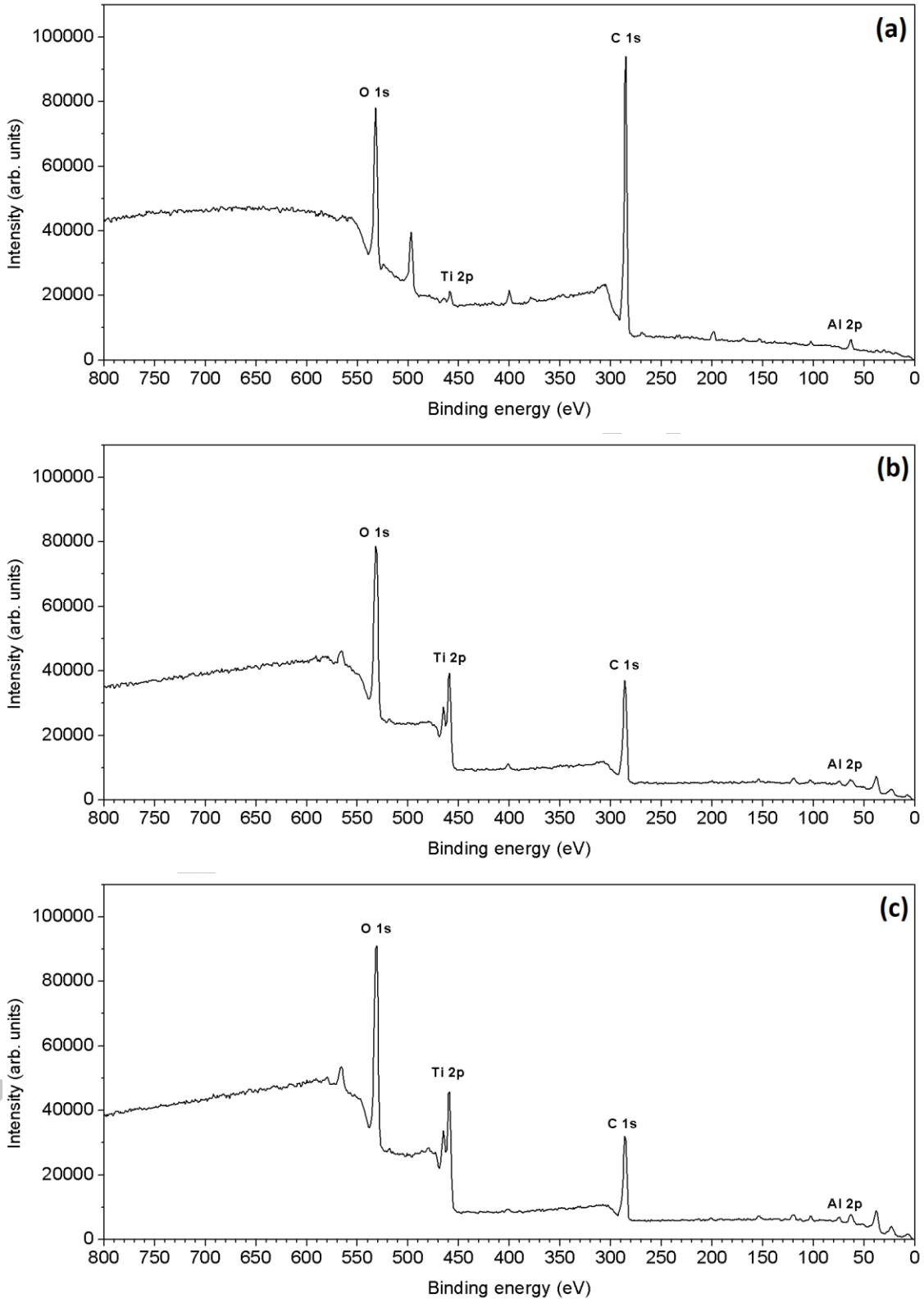

Fig. 6. XPS full spectra for (a) Ti-6Al-4V Reference sample, (b) DLW nanosecond laser patterned sample stored in air and (c) DLW nanosecond laser patterned sample stored in polyethylene bag.

Sample/Element	Reference	Air storage	Bag Storage
Ti (%)	0.93	9.64	12.36
Al (%)	0.31	2.89	3.39
C (%)	72.53	47.11	40.7
O (%)	16.57	36.81	40.35
Si (%)	0.78	1.38	1.73
S (%)	0.48	0.06	0
Cl (%)	1.1	0	0
K (%)	0.66	0	0
Na (%)	4.34	0	0
Ca (%)	0.25	0.22	0.21
N (%)	2.04	1.55	0.87
V (%)	0	0.34	0.39

Table 3. Relative surface element composition (% atomic concentration) of the unprocessed surface, an air stored DLW nanosecond laser patterned sample and a bag stored DLW nanosecond laser patterned sample.

High resolution (approx. 0.4 eV) spectra from the Ti 2*p*, Al 2*p*, C 1*s* and O 1*s* regions are shown in Fig. 7. For the Al 2*p* region, all the samples shown a similar behavior; before and after the laser treatment the spectra show peaks at 74.6 eV and 75.0 eV corresponding to aluminum oxide (Al_2O_3) doublets, Al $2p_{3/2}$ and Al $2p_{1/2}$, respectively. No trace of metallic Al (expected at 72.6 eV) were observed, suggesting that all of the Al detected was at the surface and thus prone to oxidation. For the case of the Ti 2*p* region, the reference sample exhibits a very small peak doublet corresponding to titanium oxide (TiO_2), attenuated by the layer of atmospheric contaminants on the surface. This may be related to oxidation due to the water molecules in the ambient air, and no traces of metallic Ti were observed. After the laser processing, the surface of the sample exhibits a more intense Ti 2*p* signal due to the removal of contaminants from the surface. The peaks at 459.2 eV and 465.0 eV correspond to the Ti $2p_{3/2}$ and Ti $2p_{1/2}$ titanium oxide (TiO_2) doublet, indicating that the surface of the processed area is oxidized. Again, no evidence of metallic Ti was found, indicating a TiO_2 film of thickness greater than 6 nm. Evidence for the formation of TiO_2 was corroborated by examining the O 1*s* spectra in Fig. 7, which clearly show an increase in the TiO_2 component at 530.7 eV in the processed samples. Four other components are present in the deconvolution, corresponding to aluminum oxide (Al_2O_3) and carbonyl groups (C=O) at 532.0 eV, O-C bonds and silica (SiO_2), atmospheric oxygen-containing compounds, and water molecules (H_2O). These spectra clearly show an increase in the relative amounts of TiO_2 compared to other compounds during the laser processing, but very little difference between the sample storage conditions.

Because of the laser irradiation, some contaminants that were on the surface prior the laser process had been removed, consequently reducing the contribution of O-C/SiO_2 bonds, other oxygen-containing

atmospheric contaminants, and H_2O molecules at 532.8 eV, 534.0 eV and 534.5 eV respectively. Furthermore, it also can be observed that for the polyethylene bag stored sample, the water molecules content has decreased to zero after the laser processing while exhibiting the highest SCA value, therefore, the removal of the H_2O molecules contribution to the O 1*s* peak can be attributed to the highly water-repellency observed on the sample stored in the polyethylene bag. Kietzig *et al.* has reported that a CO_2 environment is beneficial for a faster increase in the contact angle of laser patterned metallic samples due to absence of H_2O traces, furthermore, laser processed samples stored in water after the laser process never reach a hydrophobic state [34], which endorse our results found for polyethylene storage showing that an absence of water molecules is a key factor for the hydrophilic-to-hydrophobic transition.

Turning to the C 1*s* spectra in Fig. 7, the deconvolution of the data from the reference sample show four different carbon bonding environments: carbon-carbon (C-C) bonds and hydrocarbons species (C-H) at 286.1 eV, carbon-oxygen bonds (C-O) at 287.8 eV, carbonyl bonds (C=O) at 289.3 eV and carboxyl species (O=C-O) at 290.1 eV. After laser irradiation, the C-C/C-H peak is greatly reduced, due to the removal of surface contaminants during the laser ablation process. A chemical shift of 0.5 eV following the laser processing was observed and is attributed to the change in the surface potential as a result of the removal of a proportion of the hydrocarbon contaminants and the increase in the relative amount of metallic oxides at the surface. For the processed samples, the intensity of the C=O and O=C-O components was reduced to a near-negligible level. However, the C-O component only showed a reduction for the sample stored in the bag after laser processing, suggesting that the laser processing does indeed remove C-O but that the resulting surface is prone to subsequent C-O adsorption from the atmosphere. Carbon-oxygen bonds (C-O), carbonyl bounds (C=O) and O=C-O species are all polar molecules, which are related to a hydrophilic effect on wet surfaces due to the polarity of water molecules, whereas C-C and C-H bounds are non-polar and are related to the hydrophobicity of the material. This is in accordance with the results obtained for the two different storage conditions, as the sample with the highest static contact angle, i.e., more hydrophobic behavior, was the sample stored in the polyethylene bag. The XPS data show that, after 1 month of storage in a polyethylene bag, the contribution of the different polar carbon molecules found on the other two samples (reference and air stored) are almost negligible to the total chemistry composition of the surface, with the non-polar carbon molecules (C-C and C-H) the principal contributors. The XPS results suggest that the observed change in wettability can be attributed to a certain extend to the absences of carbon polar compounds, as well as H_2O molecules, as they were not detected on the sample with the highest SCA.

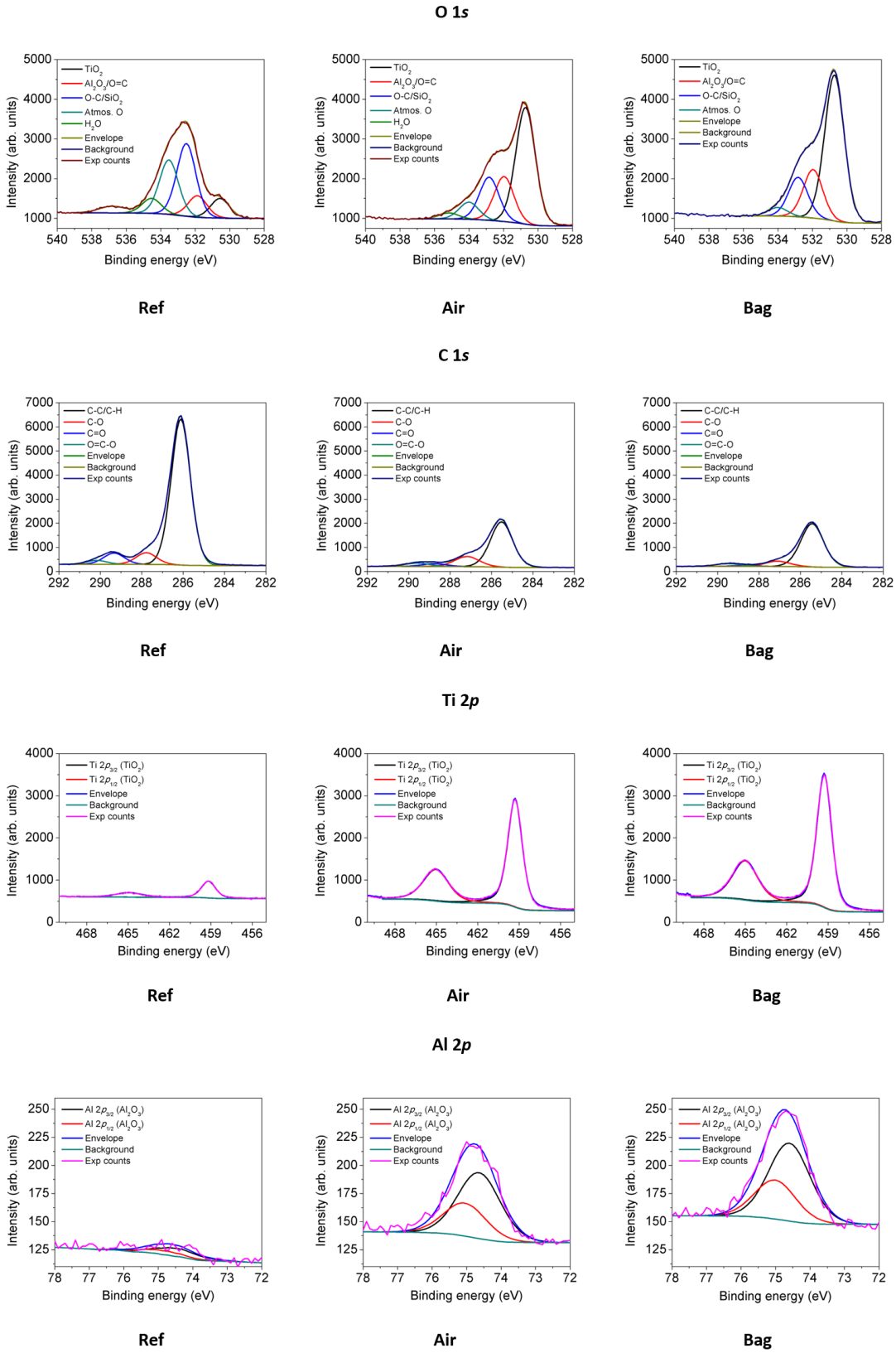

Fig. 7. High resolution (approx. 0.4 eV) spectra from the O 1*s*, C 1*s*, Ti 2*p* and Al 2*p* regions showing the different compounds.

Conclusions

Dual-scale periodic surface patterns were fabricated on Ti-6Al-4V alloy combining two laser micro-structuring techniques. Nanosecond-pulsed direct laser writing (DLW) has been employed on a high strength titanium alloy (Ti-6Al-4V) in order to create micro-pillars (20 µm in width, 2-4 µm high and depth from the original surface). Due to the dominant nanosecond thermal ablation process, a high occurrence of melting was found in the periphery of the laser tracks, leading to the development of micro-walls on top of the pillars. The resulting surface structure was a periodic array of squared micro-pillars, regularly distributed on the processed surface. Subsequently, femtosecond low spatial frequency LIPSS were generated on top of the nanosecond patterned structure to create a dual-scale structure. The femtosecond process is free of thermal effects, meaning that the previously fabricated structures were not affected by this second laser process. The LIPSS generated show self-organized ripples in a very uniform manner with a spatial period of approximately 810 nm. The final surface exhibits a dual-scale roughness thus providing a method to successfully generate hierarchical structures.

Furthermore, two storage conditions, air and polyethylene bags, were used for keeping the samples after the laser process to evaluate the aging process of the samples. Static Contact Angle measurements were made to obtain an analysis on the wettability behavior of the structures created under the two storage conditions. The non-processed surface recorded a SCA of approximately 70°, without any significant change due to the storage conditions. After one month of storage, nanosecond processed samples kept in the polyethylene bag showed a clear shift away from hydrophilic behavior and achieving a hydrophobic effect, reaching values over 150°. For the dual-scale hierarchical structures, SCA values showed an increase against the non-hierarchical structures, either kept on air or polyethylene bags, demonstrating that a hierarchical roughness is more prone to achieve a better hydrophobic state. Nevertheless, the hierarchical surfaces kept in polyethylene bags showed a higher SCA, over 160°, in comparison with the hierarchical surfaces kept on air which showed a SCA around 120°. The surface topography was the same for both samples, therefore, the change in SCA values between the two storage conditions must be also related to a change in the chemical composition of the surfaces.

XPS results showed that the laser patterned samples were heavily oxidized, with the processed samples exhibiting a clear increase in the total oxygen concentration in comparison with the reference sample. It was found that the process samples were covered by the metallic oxides TiO_2 and Al_2O_3, as well as other oxygen-containing compounds and hydrocarbons. Among the oxygen compounds, a clear difference in the relative content of water molecules between samples with the same surface structure kept in two different storage conditions was observed. For the case of the sample kept in air, water molecules were detected on the deconvolution of the O 1*s* peak, while for the case of the polyethylene bag, which shows the highest SCA, no traces of H_2O molecules were found. Furthermore, the C 1*s* peak of the XPS spectra showed that a reduction on the carbon concentration took place after the laser processing. The detailed analysis of the C 1*s* spectra for the processed samples showed traces of several polar and non-polar carbon compounds, with the sample kept in polyethylene bag showing the lowest concentration of polar molecules while also displaying the highest SCA. The results indicate that the absence of polar molecules highly affect the wettability of the surface.

These results indicate that a change on the surface roughness will improve the wettability of the surface, but it will also be necessary a change on the chemical composition of the surface which can be

influenced by the storage conditions after the laser process. While the process responsible of the transition from hydrophilic to hydrophobic is complex and still not completely clear, this research illustrated that aging of laser-textured samples in simple polyethylene bags can lead to higher water contact angles values, overall hastening the transition between hydrophilic and hydrophobic.

Acknowledgments

This work was carried out in the framework of the LASER4FUN project (http://www.laser4fun.eu), which has received funding from the European Union's Horizon 2020 research and innovation programme under the Marie Skłodowska-Curie grant agreement No 675063.

References

[1] H. Ghiradella, W. Radigan, Collembolan cuticle: Wax layer and antiwetting properties, J. Insect Physiol. 20 (1974) 301–306. doi:10.1016/0022-1910(74)90062-6.

[2] H. Gao, X. Wang, H. Yao, S. Gorb, E. Arzt, Mechanics of hierarchical adhesion structures of geckos, Mech. Mater. 37 (2005) 275–285. doi:10.1016/j.mechmat.2004.03.008.

[3] N.A. Patankar, Mimicking the lotus effect: Influence of double roughness structures and slender pillars, Langmuir. 20 (2004) 8209–8213. doi:10.1021/la048629t.

[4] Y.T. Cheng, D.E. Rodak, Is the lotus leaf superhydrophobic?, Appl. Phys. Lett. 86 (2005) 1–3. doi:10.1063/1.1895487.

[5] C.W. Extrand, S.I. Moon, Repellency of the lotus leaf: Contact angles, drop retention, and sliding angles, Langmuir. 30 (2014) 8791–8797. doi:10.1021/la5019482.

[6] A.M. Peters, C. Pirat, M. Sbragaglia, B.M. Borkent, M. Wessling, D. Lohse, R.G.H. Lammertink, Cassie-Baxter to Wenzel state wetting transition: Scaling of the front velocity, Eur. Phys. J. E. 29 (2009) 391–397. doi:10.1140/epje/i2009-10489-3.

[7] W. Choi, A. Tuteja, J.M. Mabry, R.E. Cohen, G.H. McKinley, A modified Cassie-Baxter relationship to explain contact angle hysteresis and anisotropy on non-wetting textured surfaces, J. Colloid Interface Sci. 339 (2009) 208–216. doi:10.1016/j.jcis.2009.07.027.

[8] A.J.B. Milne, A. Amirfazli, The Cassie equation: How it is meant to be used, Adv. Colloid Interface Sci. 170 (2012) 48–55. doi:10.1016/j.cis.2011.12.001.

[9] G. Whyman, E. Bormashenko, T. Stein, The rigorous derivation of Young, Cassie-Baxter and Wenzel equations and the analysis of the contact angle hysteresis phenomenon, Chem. Phys. Lett. 450 (2008) 355–359. doi:10.1016/j.cplett.2007.11.033.

[10] S. Peng, B. Bhushan, Mechanically durable superoleophobic aluminum surfaces with microstep and nanoreticula hierarchical structure for self-cleaning and anti-smudge properties, J. Colloid Interface Sci. 461 (2016) 273–284. doi:10.1016/j.jcis.2015.09.027.

[11] Z. Chen, L. Hao, C. Chen, A fast electrodeposition method for fabrication of lanthanum superhydrophobic surface with hierarchical micro-nanostructures, Colloids Surfaces A Physicochem. Eng. Asp. 401 (2012) 1–7. doi:10.1016/j.colsurfa.2012.02.020.

[12] B. Bhushan, K. Koch, Y.C. Jung, Biomimetic hierarchical structure for self-cleaning, Appl. Phys. Lett. 93 (2008) 1–4. doi:10.1063/1.2976635.

[13] Y. Zhou, Q. Bao, B. Varghese, L.A.L. Tang, C.K. Tan, C.H. Sow, K.P. Loh, Microstructuring of graphene oxide nanosheets using direct laser writing, Adv. Mater. 22 (2010) 67–71. doi:10.1002/adma.200901942.

[14] J.-H. Yoo, H.-J. Kwon, D. Paeng, J. Yeo, S. Elhadj, C.P. Grigoropoulos, Facile fabrication of a superhydrophobic cage by laser direct writing for site-specific colloidal self-assembled photonic crystal, Nanotechnology. 27 (2016) 145604. doi:10.1088/0957-4484/27/14/145604.

[15] S. Razi, K. Madanipour, M. Mollabashi, Laser surface texturing of 316L stainless steel in air and water: A method for increasing hydrophilicity via direct creation of microstructures, Opt. Laser Technol. 80 (2016) 237–246. doi:10.1016/j.optlastec.2015.12.022.

[16] J.T. Cardoso, A. Garcia-Girón, J.M. Romano, D. Huerta-Murillo, R. Jagdheesh, M. Walker, S.S. Dimov, J.L. Ocaña, Influence of ambient conditions on the evolution of wettability properties of an IR-, ns-laser textured aluminium alloy, RSC Adv. 7 (2017) 39617–39627. doi:10.1039/C7RA07421B.

[17] C. Ma, S. Bai, Y. Meng, X. Peng, Hydrophilic control of laser micro-square-convexes SiC surfaces, Mater. Lett. 109 (2013) 316–319. doi:10.1016/j.matlet.2013.07.097.

[18] G. (G R.B.E. Romer, M. Jorritsma, D. Arnaldo Del Cerro, B. Chang, V. Liimatainen, Q. Zhou, B. (A J. Huis in 't Veld, Laser micro-machining of hydrophobic-hydrophilic patterns for fluid driven self-alignment in micro-assembly, LPM_International Symp. Laser Precis. Microfabr. (2011) 10. http://doc.utwente.nl/79554/.

[19] R. Jagdheesh, J.L. Ocaña, One-Step Generation of Ultrahydrophobic Aluminum Surface Patterns by Nanosecond Lasers, Proceeding LIM. (2015).

[20] U. Trdan, M. Hočevar, P. Gregorčič, Transition from superhydrophilic to superhydrophobic state of laser textured stainless steel surface and its effect on corrosion resistance, Corros. Sci. 123 (2017) 21–26. doi:10.1016/j.corsci.2017.04.005.

[21] L.B. Boinovich, A.M. Emelyanenko, A.D. Modestov, A.G. Domantovsky, K.A. Emelyanenko, Synergistic Effect of Superhydrophobicity and Oxidized Layers on Corrosion Resistance of Aluminum Alloy Surface Textured by Nanosecond Laser Treatment, ACS Appl. Mater. Interfaces. 7 (2015) 19500–19508. doi:10.1021/acsami.5b06217.

[22] A.M. Emelyanenko, F.M. Shagieva, A.G. Domantovsky, L.B. Boinovich, Nanosecond laser micro- and nanotexturing for the design of a superhydrophobic coating robust against long-term contact with water, cavitation, and abrasion, Appl. Surf. Sci. 332 (2015) 513–517. doi:10.1016/j.apsusc.2015.01.202.

[23] V.D. Ta, A. Dunn, T.J. Wasley, J. Li, R.W. Kay, J. Stringer, P.J. Smith, E. Esenturk, C. Connaughton, J.D. Shephard, Laser textured superhydrophobic surfaces and their applications for homogeneous spot deposition, Appl. Surf. Sci. 365 (2016) 153–159. doi:10.1016/j.apsusc.2016.01.019.

[24] R. Jagdheesh, M. Diaz, J.L. Ocaña, Bio inspired self-cleaning ultrahydrophobic aluminium surface by laser processing, RSC Adv. 6 (2016) 72933–72941. doi:10.1039/c6ra12236a.

[25] L.R. de Lara, R. Jagdheesh, J.L. Ocaña, Corrosion resistance of laser patterned ultrahydrophobic

aluminium surface, Mater. Lett. 184 (2016) 100–103. doi:10.1016/j.matlet.2016.08.022.

[26] J. Long, P. Fan, M. Zhong, H. Zhang, Y. Xie, C. Lin, Superhydrophobic and colorful copper surfaces fabricated by picosecond laser induced periodic nanostructures, Appl. Surf. Sci. 311 (2014) 461–467. doi:10.1016/j.apsusc.2014.05.090.

[27] A.Y. Vorobyev, C. Guo, Multifunctional surfaces produced by femtosecond laser pulses, J. Appl. Phys. 117 (2015) 1–6. doi:10.1063/1.4905616.

[28] A.M. Kietzig, S.G. Hatzikiriakos, P. Englezos, Ice friction: The effects of surface roughness, structure, and hydrophobicity, J. Appl. Phys. 106 (2009). doi:10.1063/1.3173346.

[29] D. Huerta-Murillo, A.I. Aguilar-Morales, S. Alamri, J.T. Cardoso, R. Jagdheesh, A.F. Lasagni, J.L. Ocaña, Fabrication of multi-scale periodic surface structures on Ti-6Al-4V by direct laser writing and direct laser interference patterning for modified wettability applications, Opt. Lasers Eng. 98 (2017). doi:10.1016/j.optlaseng.2017.06.017.

[30] C. Kunz, T.N. Büttner, B. Naumann, A. V. Boehm, E. Gnecco, J. Bonse, C. Neumann, A. Turchanin, F.A. Müller, S. Gräf, Large-area fabrication of low- and high-spatial-frequency laser-induced periodic surface structures on carbon fibers, Carbon N. Y. 133 (2018) 176–185. doi:10.1016/j.carbon.2018.03.035.

[31] Y.C. Guan, F.F. Luo, G.C. Lim, M.H. Hong, H.Y. Zheng, B. Qi, Fabrication of metallic surfaces with long-term superhydrophilic property using one-stop laser method, Mater. Des. 78 (2015) 19–24. doi:10.1016/j.matdes.2015.04.021.

[32] J. Long, M. Zhong, H. Zhang, P. Fan, Superhydrophilicity to superhydrophobicity transition of picosecond laser microstructured aluminum in ambient air, J. Colloid Interface Sci. 441 (2015) 1–9. doi:10.1016/j.jcis.2014.11.015.

[33] D.M. Chun, C.V. Ngo, K.M. Lee, Fast fabrication of superhydrophobic metallic surface using nanosecond laser texturing and low-temperature annealing, CIRP Ann. - Manuf. Technol. 65 (2016) 519–522. doi:10.1016/j.cirp.2016.04.019.

[34] A.M. Kietzig, S.G. Hatzikiriakos, P. Englezos, Patterned superhydrophobic metallic surfaces, Langmuir. 25 (2009) 4821–4827. doi:10.1021/la8037582.

[35] J.M. Romano, A. Garcia-Giron, P. Penchev, S. Dimov, Triangular laser-induced submicron textures for functionalising stainless steel surfaces, Appl. Surf. Sci. 440 (2018) 162–169. doi:10.1016/j.apsusc.2018.01.086.

Highlights

- Square micro-structures were fabricated with nanosecond laser pulses in Ti-6Al-4V.
- LIPSS with a spatial period of 810 nm were created in top of the prior structures.
- Air and polyethylene storage conditions were used to analyze aging and wettability.
- Hierarchical structures were hydrophobic with SCA over 160° for polyethylene.
- Hydrophobic surface had the lower concentration of polar molecules.

Graphical abstract